Supplementary Materials for

Thallium isotopes reveal protracted anoxia during the Toarcian (Early Jurassic) associated with volcanism, carbon burial, and mass extinction

Theodore R. Them II, Benjamin C. Gill, Andrew H. Caruthers, Angela M. Gerhardt, Darren R. Gröcke, Timothy W. Lyons, Selva M. Marroquín, Sune G. Nielsen, João P. Trabucho Alexandre, and Jeremy D. Owens

correspondence to: themtr@cofc.edu

This PDF file includes:

Other Supplementary Materials for this manuscript includes the following:

www.pnas.org/cgi/doi/10.1073/pnas.1803478115

Materials and Methods

Sampling Locations and Materials

Published accounts of the collective lithostratigraphy, ammonite biostratigraphy, U-Pb zircon age dates, and high-resolution carbon isotope chemostratigraphy for the East Tributary and Dotternhausen Quarry can be found in refs. 1, 2, 3, 4. Here, we discuss and summarize key aspects of these analyses as they pertain to our study.

Drill cores 1-35-62-20W5 and 6-32-78-5W6 (SI Figs. 1, 2) of the Fernie Formation were described and sampled for geochemical analyses at the Core Research Centre in Calgary, Alberta, Canada. They contain the Pliensbachian to lower Toarcian Gordondale and Poker Chip Shale (PCS) members, and have been correlated by geophysical gamma ray logs, ammonites, and carbon isotopes to outcrops of Red Deer and PCS, including East Tributary (1, 5, 6). Each core contains mixed organic-rich calcareous mudstones and siltstones in the Gordondale Member, which are overlain by organic-rich calcareous mudstones of the PCS (5).

Core 1-35-62-20W5 contains alternating organic-rich calcareous siltstones and mudstones (SI Fig. 1) of the Gordondale and PCS members. The Gordondale Member ranges from the base of the core to 2029 m and contains several bivalve beds (5) and the Pliensbachian (Freboldi Zone) ammonite *Dubariceras* cf. *silviesi* at 2033.3 m. The PCS Member comprises 2029 m to the top of the core (5) and contains organic-rich calcareous mudstones, displacive and diagenetic carbonate cements and fans, with abundant bivalves, the cephalopod *Actractites*, and the Toarcian ammonite Dactylioceras sp. at 2027.1 m (5).

Core 6-32-78-5W6 contains alternating organic-rich calcareous siltstones and mudstones (SI Fig. 2) of the Gordondale and PCS members. The Gordondale Member ranges from the base of the core to ~1219 meters (5) and contains several bivalve beds[5], the Pliensbachian ammonite *Amaltheus* sp. at 1221.8 m, and Toarcian Kanense to Planulata Zone equivalent *Dactylioceras cf. crosbeyi* and *Cleviceras exaratum* at 1217.9 and 1217.8 meters, respectively. From 1221 to 1219 m, the dominant lithology is an organic-rich mudstone, with a thin, organic-rich, silty mudstone capped by a displacive carbonate fan around 1220.25 m. From 1219 to 1214.6 m, the dominant lithology is an organic-rich, laminated, calcareous siltstone, with many bitumen-rich intervals. The PCS Member comprises 1214.6 m to the top of the core (5) and contains organic-rich calcareous mudstones, rare bivalves, and often contains intervals that are laminated.

These sections represent an excellent opportunity to use the Toarcian CIE as an intra-basinal and a global chemostratigraphic marker (SI Fig. 3); since these cores represent time-correlative, deeper-water facies to the East Tributary section (5), it is possible to reconstruct paleoceanographic dynamics across the T-OAE. Specifically, if redox variations change with paleo-water depth, and potentially temporally, then it should be possible to reconstruct the temporal and spatial extent of oxygenation within the basin.

Total organic carbon contents (TOC) and isotope compositions ($\delta^{13}C_{org}$)

Carbon-isotope and total organic carbon content data of the East Tributary and Dotternhausen sites were recently reported by refs. 1, 2 and ref. 4, respectively. The new data presented here are from the 1-35-62-20W5 and 6-32-78-5W6 drill cores and follow the methods in refs. 1, 2, 4.

Powders were obtained from the drill core and outcrops samples either using a handheld Dremel tool with a diamond tip drill bit or a ball mill using a silica nitride ceramic vial set. To remove the carbonate fraction, several milliliters of 2N HCl were added to ~0.1 g of powder and allowed to react for ~24 hours. The solution was rinsed until a neutral pH was obtained, and then the samples were dried in an oven.

$\delta^{13}C_{org}$ and total organic carbon (TOC) values of the carbonate-free sample residues were conducted on an Isotope Cube elemental analyzer connected to an Isoprime 100 gas source isotope-ratio mass spectrometer (IRMS) in the Sedimentary Geochemistry Isotope Laboratory in the Department of Geosciences at Virginia Tech. The isotope compositions of the samples were expressed in the standard delta (δ) notation as per mil deviations (‰) from Vienna Pee Dee Belemnite (VPDB) and calculated such that:

$$\delta^{13}C=[((^{13}C/^{12}C)_{sample} - (^{13}C/^{12}C)_{standard}) / (^{13}C/^{12}C)_{standard}] \times 1000 \qquad \textbf{Eq. 1}$$

Samples were calibrated to the VPDB scale using international (IAEA-CH-6 and IAEA-CH-7) and commercial standards (Elemental Microanalysis wheat flour, sorghum flour, low organic soil, and urea). Long-term analytical precision for the $\delta^{13}C$ measurements is <0.1‰ based on replicated analyses on isotope standards: this provided a linear range in $\delta^{13}C$ between -48.66‰ and -10.42‰. Total organic carbon was obtained as part of the isotopic analysis using elemental standards (i.e., Acetanilide, 71.09% C). Approximately 66% of total samples (n = 86) from core 6-32-78-5W6 were replicated at least once. Approximately 91% of total samples (n = 78) from core 1-35-62-20W5 were replicated at least once. Average analytical uncertainty for replicated analyses (n = 128) was 0.07‰.

Iron speciation analysis

The amount of iron found in various mineral phases (iron speciation) of fine-grained siliciclastic units can be used to identify local modern and ancient water column redox conditions (7-10). Specifically, the amount highly reactive iron-bearing phases (Fe_{HR}; see Equation 2) can be quantified to determine local redox conditions during deposition (11). The Fe_{HR} pool represents available iron that reacts with aqueous sulfide to form pyrite (12). The highly reactive iron pool (e.g., 10) is defined as:

$$Fe_{HR} = Fe_{py} + Fe_{carb} + Fe_{ox} + Fe_{mag} \qquad \textbf{Eq. 2}$$

where Fe_{py} represents iron bound as pyrite; Fe_{carb} represents iron hosted in carbonate phases including calcite, siderite, and ankerite; Fe_{ox} represents iron hosted in the ferrihydrite, lepidocrocite, goethite, and hematite fractions; and Fe_{mag} represents iron hosted in the magnetite fraction.

Modern and ancient marine siliciclastic sediments deposited under an anoxic water column have a Fe_{HR}/Fe_T (Fe_T represents total iron in the sample) value of >0.38, whereas sediments deposited under an oxic water column are generally below 0.22 (7, 11, 13). Because the amount of pyrite that can be deposited in anoxic environments during the microbial reduction of sulfate (e.g., 12) can vary, the amount of Fe_{py} to Fe_{HR} in each sample can help discern whether the water column was ferruginous (pyrite formation limited by available sulfides) or euxinic (pyrite formation limited by available reactive

iron). Fe_{py}/Fe_{HR} values > ~0.7-0.8 are indicative of water column euxinia, whereas Fe_{py}/Fe_{HR} values < ~0.7-0.8 are indicative of ferruginous conditions (11, 14, 15).

To determine the relative amount of iron in each iron-bearing phase, the sequential extraction method of ref. 8 was performed at the Department of Geosciences at Virginia Tech. For this procedure, approximately 0.1 grams of powder was used. First, Fe_{carb} was liberated by the addition of a 10mL solution of 1M sodium acetate and acetic acid, buffered to pH of 4. These samples were placed on a shaking table for 48 hours at 50° C and then centrifuged. Next, Fe_{ox} was liberated from the samples by the addition of a 10mL solution of sodium dithionite and sodium citrate, buffered to pH of 4. These samples were placed on a shaking table for two hours, and then centrifuged. Finally, Fe_{mag} was liberated by the addition of a 10mL solution of ammonium oxalate. These samples were placed on a shaking table for six hours, and then centrifuged. After each extraction, 100 μL of the supernatant was transferred to a new tube, followed by the addition of 4 mL of HEPES, ferrozine, and hydroxylamine HCl solution (e.g., 16) and allowed to react overnight. All of the supernatant was removed in the original sample tubes before the next iron extraction. Iron concentrations were measured in a spectrophotometer and calculated by a matrix-matched standard curve (e.g., 17).

Fe_{py} values were determined by chromium reduction methods of ref. 18. For this procedure, approximately 0.1 grams of powder was added to a three-neck flask for a distillation extraction. Following the purging of headspace with nitrogen gas a solution of 40 mL of 1M chromous chloride and 20 mL of 6N HCl was added to the flask, and then allowed to react for two hours while heating under the nitrogen atmosphere. Any volatized sulfide quantitatively reacted with a zinc acetate solution to form zinc sulfide. Later, silver nitrate was added to this solution, which converted the zinc sulfide to silver sulfide. The amount of sulfide in the sample was then determined by gravimetry after filtration and drying of the silver sulfide. The amount of pyrite iron hosted in the original sample was then stoichiometrically calculated from the amount of extracted sulfide.

For the determination of Fe_T approximately 0.2 grams of powder was ashed at 900° C for 6-8 hours to remove any organic matter and other volatile phases. Approximately 0.1 grams of powder was partially dissolved using 4 mL of 12M HCl, and then placed in a trace metal clean Teflon Savillex digestion vessel on a hot plate and boiled for 36-48 hours (19). The sample and solution were added to centrifuge tubes and centrifuged. After centrifugation, 100 μL of the supernatant was transferred to a new tube and the same technique was used to measure iron concentrations using a spectrophotometer as stated previously.

Iron concentrations were calculated by a matrix-matched standard curve. New standard solutions were prepared for each analysis with iron standard concentrations at 0, 5, 10, 20, 30, 40 75, 150, and 300 ppm. The r^2 value of the standard curve was always above 0.999 and many instances was 1. Multiple analyses of the same solution yielded no error via spectrophotometer output, and no samples yielded higher iron concentrations than the standards. Sample reproducibility using this method is often ± 7% when analyzing different aliquots of the same extracted iron pool (e.g., 17).

Thallium isotope analysis

The precipitation of manganese oxides is directly controlled by available oxygen, and therefore ceases in low oxygen environments. As manganese oxide precipitation

decreases during the onset of widespread deoxygenation in the oceans, changes the Tl elemental and isotopic budget are the first systems to be perturbed (20). To assess the global dynamics of oceanic oxygenation during the Early Jurassic, this study utilizes a novel isotopic system that is not fractionated by biological processes in the open ocean (*23*). Thallium has two naturally occurring isotopes: ^{203}Tl and ^{205}Tl. The thallium isotopic composition of a sample is compared to the NIST SRM 997 Tl standard and reported such that:

$$\varepsilon^{205}Tl = 10{,}000 \times (^{205}Tl/^{203}Tl_{sample} - ^{205}Tl/^{203}Tl_{SRM\ 997}) / (^{205}Tl/^{203}Tl_{SRM\ 997}) \quad \textbf{Eq. 3}$$

To track manganese oxide burial during the Early Jurassic, chemical analysis (21, 22) was utilized to isolate thallium in a state-of-the-art clean laboratory at the National High Magnetic Field Laboratory at Florida State University. For this procedure, approximately 0.05 grams of sample powder (0.1 grams of standard SCO-1) was placed into a trace metal clean teflon savillex beaker with 3mL of 2M HNO_3 was added and placed on a hot plate for approximately 12 hours at 130° C. These samples were then centrifuged, and the supernatant was collected and placed in a new, clean savillex beaker, and dried. Care was taken to not collect siliciclastic materials, and to ensure limited siliciclastic Tl contamination HF was avoided. Several high-purity acid treatments (aqua regia, 50% conc. HCl or HNO_3 + H_2O_2) were added to each beaker to fully oxidize any organic matter present. These solutions were placed on hot plates at 120-130° C for several days if necessary. To completely oxidize samples for column chemistry, 1 M HCl and ~100 μL brominated H_2O were added to each beaker the previous night. All acids and reagents were trace metal grade to ensure low blank levels.

For column chemistry, we followed the method of refs. 23-25 (described below), but this dataset only used one micro-column procedure, which was shown to work well for high Tl and low Pb samples (22). For Pb removal, AG1X8 200-400 mesh resin was added to each column. This was followed by the addition of solutions 0.1 ml and 1.5 ml of each HCl-SO_2, 0.1M HCl, and 0.1 M HCl with 1% Br_2-H_2O. Samples were loaded into the columns, followed by the addition of 0.1 ml and 1.5 ml solutions of 0.5 M HNO_3 – 3% Br_2-H_2O, 2.0 M HNO_3 – 3% Br_2-H_2O, and 0.1 M HCl – 1% Br_2-H_2O. Thallium was then collected using 0.1 ml and 1.5 ml of 0.1 M HCl-SO_2 solution. Importantly, H_2SO_4 was evaporated at high temperature, and each sample was dissolved in a 0.1 M HNO_3 + 0.1% H_2SO_4 solution. A 10-μL aliquot of this solution was analyzed with an Agilent 7500cs ICP-MS to measure Pb and Tl abundances. Using these concentration data, sample concentrations were matched to within 25% of standard and spiked with an abundance of NIST SRM 997 Pb standard. Thallium isotope measurements were performed on a Thermo Neptune MC-ICP-MS at FSU. Approximately 90% of the samples were analyzed at least twice (some samples were not replicated due to sample limitation). The average 2σ standard deviation for all replicated samples is ± 0.25 epsilon units or better. The long-term average $\varepsilon^{205}Tl$ value for the SCo-1 standard is -2.99 ± 0.3 and all of our SCo-1 values were within this range. Samples that had reproducibility under 0.3 were displayed with an uncertainty of 0.3 (long-term reproducibility of SCo-1 standard), and samples that had reproducibility above 0.3 are displayed with that specific uncertainty.

Supplementary Text

Revised placement of Pliensbachian-Toarcian boundary at East Tributary section

The original placement of the Pliensbachian-Toarcian boundary at East Tributary was placed at ~10.15 m based on the first appearance of the Toarcian ammonites *Cleviceras exaratum* and *Hildaites cf. murleyi* (1). However, the boundary could feasibly occur between ~8.5 m and 10.15 m, as this interval also includes ammonites that are known to span the Pliensbachian-Toarcian boundary in western North America (i.e., *Tiltoniceras cf. antiquum* and *Protogrammoceras paltum* (27, 28). Regardless of boundary placement our interpretations remain consistent in that water column deoxygenation predated the large negative CIE of the T-OAE, rather occurring at the Pliensbachian-Toarcian boundary over a time-frame that is coeval with phase 3 of the multi-phased Pliensbachian-Toarcian mass extinction (29) and supported by osmium isotope geochemical records (2, 30) and the absolute ages of the Pliensbachian-Toarcian boundary (2, 31, 32). Therefore, deoxygenation would still be considered as a major driver for the main phase of this mass extinction event.

Positive carbon isotope excursion during the early Toarcian (pre-T-OAE CIE)

In Fig. 1 of the main text, the long-term, globally observed positive carbon isotope excursion during the early Toarcian is noted. This phenomenon is observed in inorganic and organic matter of marine and terrestrial carbon in several locations from Europe, Africa, and North America (1, 33-39) (Fig. S3). The new thallium isotope dataset from western Canada suggest that increased anoxia and burial of organic carbon were the mechanisms behind the long-term positive CIE beginning in the basal Toarcian.

Ammonite zones of new oceanic deoxygenation records

New Tl data from two geographically far removed anoxic basins suggest that the expansion of early Toarcian anoxic bottom began at the base of the correlative Tenuicostatum (northwest Europe and South America), Polymorphum (Mediterranean), Antiquum (High-Arctic), and Kanense (western North America) zones, and continued into the middle Toarcian at a correlative level with the Bifrons Zone of northwest Europe (see ref. 29).

Dotternhausen Quarry Tl isotopes

In Fig. 2 of the main text, several Tl isotope data points below the T-OAE CIE were displayed as light gray. These samples came from carbonate marls with extremely low TOC contents (0.34 – 0.78%) (4). Therefore, we compared only the two Tl isotope data points from the organic matter-rich black shales (pre-T-OAE) with the organic matter-rich black shales from the OAE and post-OAE interval. Interpreting the Tl-isotopic composition of the low TOC marls as a proxy for relative global manganese oxide burial is unexplored and could lead to erroneous conclusions as the Tl-isotope proxy (and other metal isotope proxies) have not been developed or tested in such depositional environments.

Yorkshire, UK Tl isotopes

The Tl-isotope results from our two new study sites cannot be directly compared with that of Yorkshire, UK (42). This is because of the interpreted severe basinal restriction that accompanied the T-OAE interval in the Cleveland Basin (43). The basinal restriction associated with this interval is demonstrated to have overprinted rhenium,

osmium, and molybdenum systems, which has resulted in isotope stratigraphies that were not indicative of the global record (2, 4, 30, 43). Furthermore, the larger variations in the Tl-isotopes at Yorkshire (42) compared to western North America and Germany (this study) suggest the record is related to regional or local Mn-oxide burial events not well connected with the open ocean.

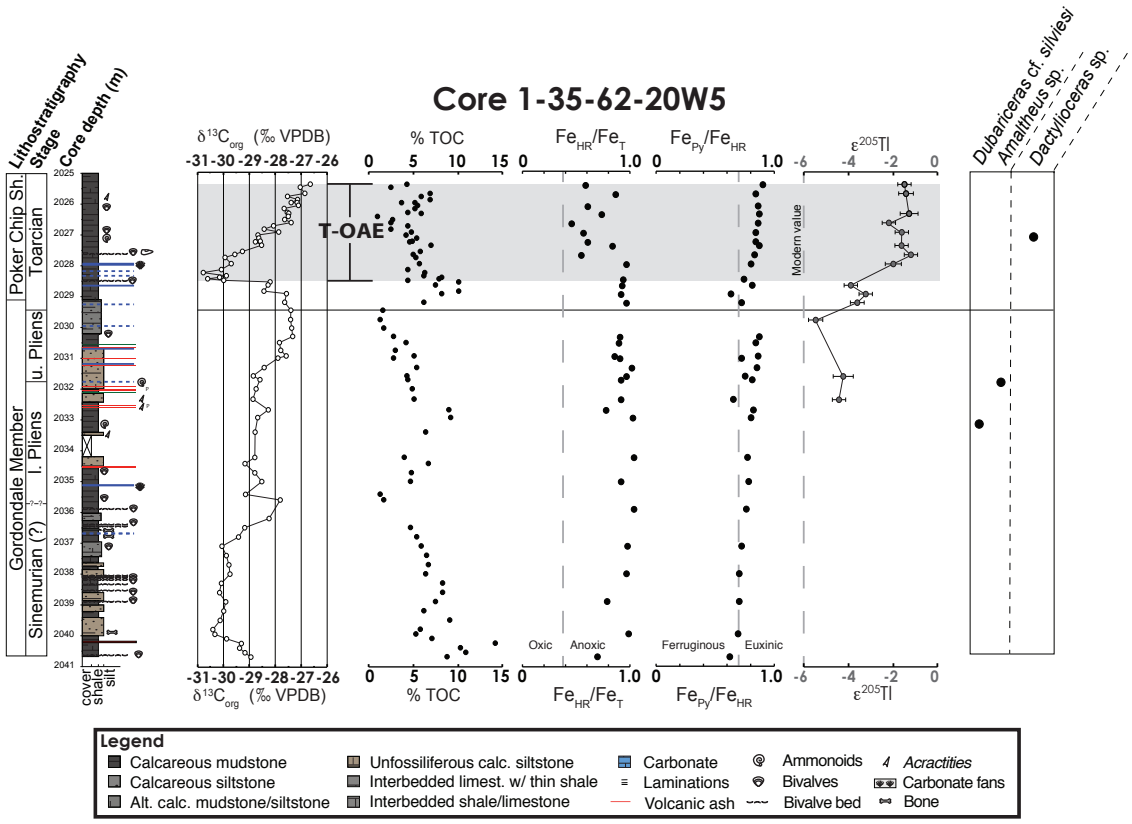

Fig. S1.

Litho- and Chemo-stratigraphies of the Lower Jurassic Fernie Formation from drill core 1-35-62-20W5, Alberta, Canada. $\delta^{13}C_{org}$ = organic carbon isotopic compositions. Fe_{HR}/Fe_T = amount of highly reactive iron relative to total iron, and Fe_{Py}/Fe_{HR} = amount of pyrite iron relative to highly reactive iron (see SI Materials and Methods for discussion of this local redox proxy). $\varepsilon^{205}Tl_{SW}$ = thallium isotopic composition of seawater during deposition. Lithostratigraphic members of the Fernie Formation and Stages of the Jurassic are shown to the left of the stratigraphic column. Gray bar represents classic T-OAE interval. Horizontal solid black line represents possible Pliensbachian/Toarcian boundary.

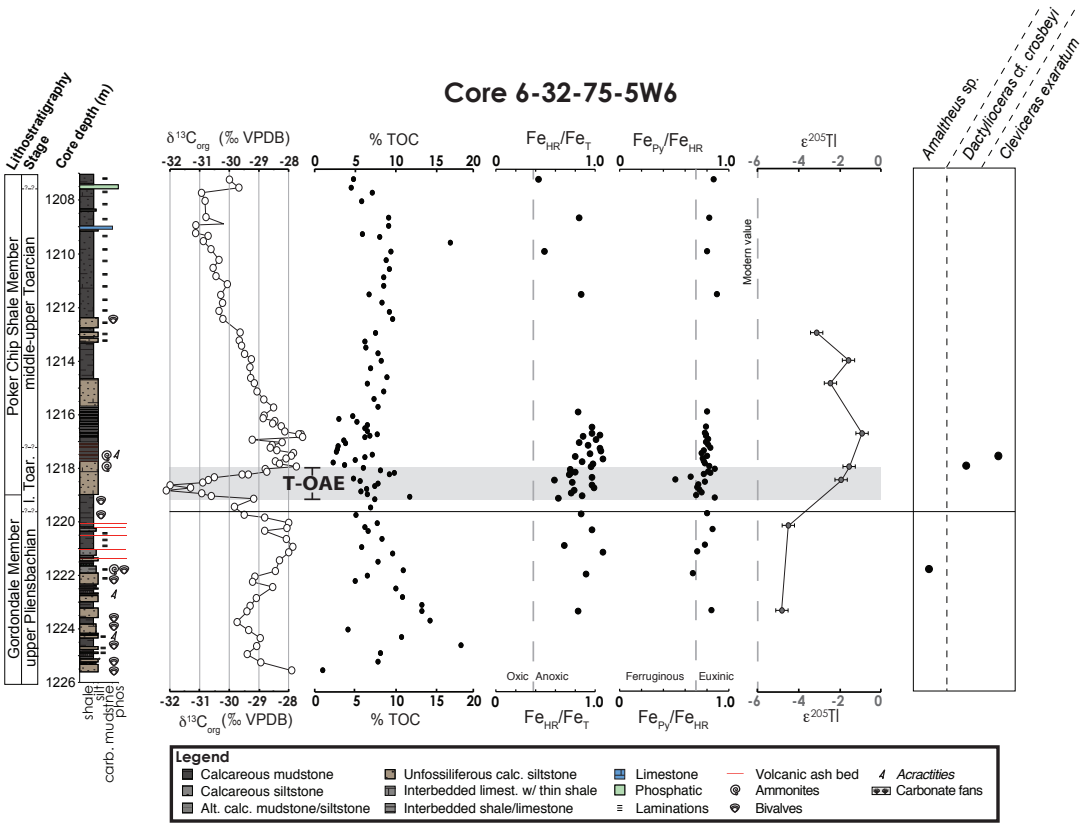

Fig. S2.

Litho- and Chemo-stratigraphies of the Lower Jurassic Fernie Formation from drill core 6-32-78-5W6, Alberta, Canada. $\delta^{13}C_{org}$ = organic carbon isotopic compositions. Fe_{HR}/Fe_T = amount of highly reactive iron relative to total iron, and Fe_{Py}/Fe_{HR} = amount of pyrite iron relative to highly reactive iron. $\varepsilon^{205}Tl_{SW}$ = thallium isotopic composition of seawater during deposition. Lithostratigraphic members of the Fernie Formation and Stages of the Jurassic are shown to the left of the stratigraphic column. Gray bar represents classic T-OAE interval. Horizontal solid black line represents possible Pliensbachian/Toarcian boundary.

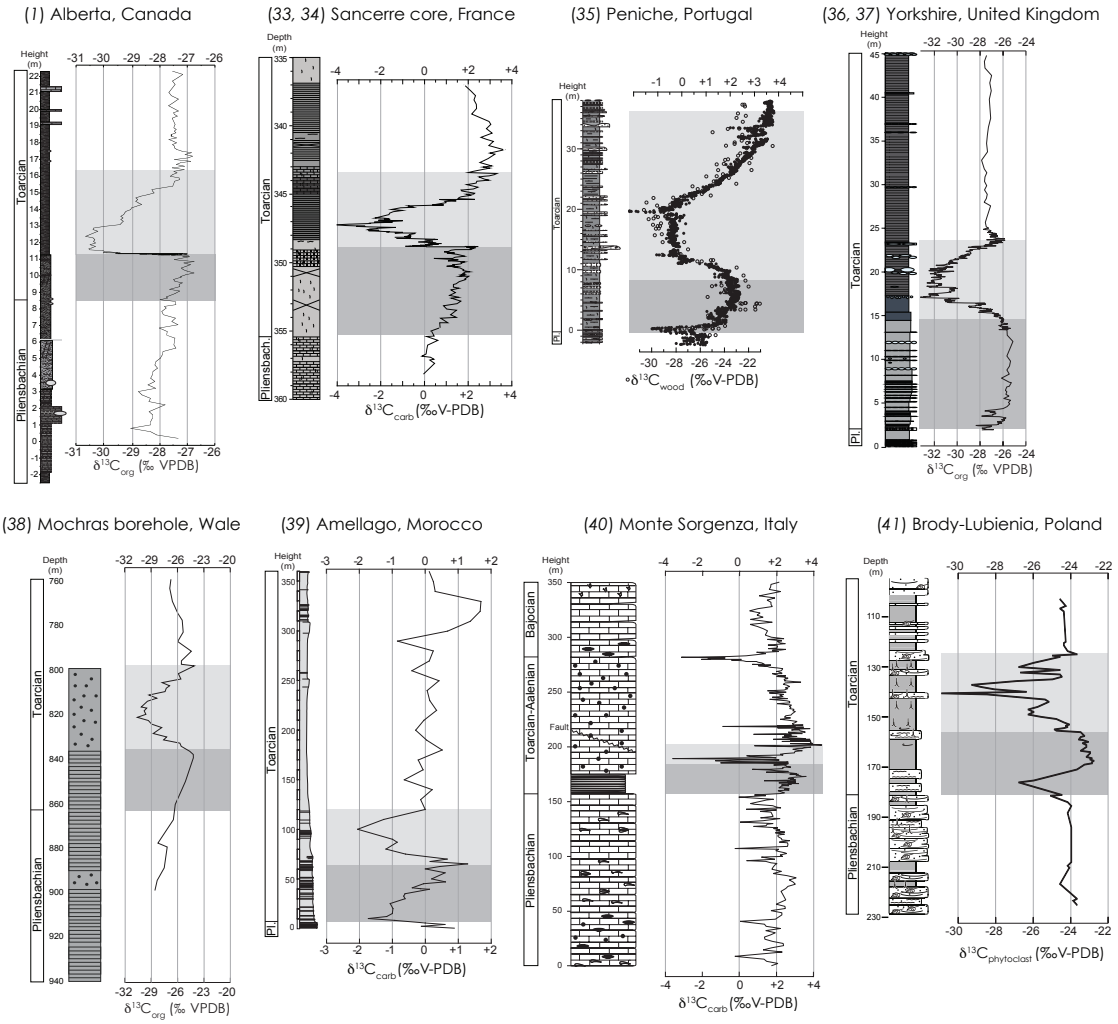

Fig. S3.

Carbon-isotope chemostratigraphies of the Pliensbachian and Toarcian stages from multiple locations. $\delta^{13}C_{org}$ = organic carbon isotopic compositions; $\delta^{13}C_{carb}$ = inorganic carbon isotopic compositions; $\delta^{13}C_{wood}$ and $\delta^{13}C_{phytoclast}$ = organic carbon isotopic compositions of terrestrial plant wood. These carbon-isotope records all display and long-term positive $\delta^{13}C$ trend in the early Toarcian until the pronounced negative CIE associated with the T-OAE (1, 33-39). Dark gray box represents this long-term positive CIE. Light gray box represents the T-OAE CIE. The Tl isotope record suggests that the increased geographical extent of anoxia increased and resulted in the burial of organic carbon (^{13}C-depleted) and ultimately the globally observed trend in higher $\delta^{13}C$ values leading up to the T-OAE.

Additional Data table S1 (separate file)

Iron speciation and thallium isotope data from the East Tributary section.

Additional Data table S2 (separate file)

Carbon isotope, total organic carbon (TOC), iron speciation, and thallium isotope data from drill core 1-35-62-20W5.

Additional Data table S3 (separate file)

Carbon isotope, total organic carbon (TOC), iron speciation, and thallium isotope data from drill core 6-32-75-5W6.

Additional Data table S4 (separate file)

Iron speciation and thallium isotope data from the Dotternhausen section.

References

1. Them TR II, et al. (2017) High-resolution carbon isotope records of the Toarcian Oceanic Anoxic Event (Early Jurassic) from North America and implications for the global drivers of the Toarcian carbon cycle. *Earth Plan Sci Lett* 459:118–126.
2. Them TR, et al. (2017) Evidence for rapid weathering response to climatic warming during the Toarcian Oceanic Anoxic Event. *Sci Rep* 7:5003.
3. Röhl H-J, Schmid-Röhl A, Oschmann W, Frimmel A, Schwark L (2001) The Posidonia Shale (Lower Toarcian) of SW-Germany: an oxygen-depleted ecosystem controlled by sea level and palaeoclimate. *Palaeogeo Palaeoclim Palaeoecol* 169:273–299.
4. Dickson AJ, et al. (2017) Molybdenum isotope chemostratigraphy and paleoceanography of the Toarcian Oceanic Anoxic Event (Early Jurassic). *Paleocean* 32:813–829.
5. Asgar-Deen M, Hall R, Craig RJ, Riediger C (2003) New biostratigraphic data from the Lower Jurassic Fernie Formation in the subsurface of west-central Alberta and their stratigraphic implications. *Can J Earth Sci* 40:45-63.
6. Hall RL, Poulton TP, Monger JWH, Field trip A1: Calgary – Vancouver in *Field Guide for the Fifth International Symposium on the Jurassic System, Vancouver*, P. L. Smith, Ed. (Jurassic Sumcomission of the Stratigraphic Commission on the International Union of Geological Sciences, Vancouver, 1998), chap. 2, pp. 29–61.
7. Poulton SW, Raiswell R (2002) The low-temperature geochemical cycle of iron: From continental fluxes to marine sediment deposition. *Amer J Sci* 302:774–805.
8. Lyons TW, Severmann S (2006) A critical look at iron paleoredox proxies: New insights from modern euxinic marine basins. *Geochim Cosmochim Acta* 70:5698–5722.
9. Canfield DE, Poulton SW, Narbonne GM (2007) Late-Neoproterozoic Deep-Ocean Oxygenation and the Rise of Animal Life. *Sci* 315:92–95.
10. Poulton SW, Canfield DE (2005) Development of a sequential extraction procedure for iron: implications for iron partitioning in continentally derived particulates. *Chem Geol* 214:209–221.
11. Poulton SW, Canfield DE (2011) Ferruginous conditions: A dominant feature of the ocean through Earth's history. *Elem* 7:107–112.
12. Berner RA (1984) Sedimentary pyrite formation: An update. *Geochim Cosmochim Acta* 48:605–615.
13. Raiswell R, Newton R, Wignall PB (2001) An Indicator of Water-Column Anoxia: Resolution of Biofacies Variations in the Kimmeridge Clay (Upper Jurassic, U.K.). *J Sed Res* 71:286–294.
14. März C, Poulton SW, Beckmann B, Küster K, Wagner T, Kasten S (2008) Redox sensitivity of P cycling during marine black shale formation: Dynamics of sulfidic and anoxic, non-sulfidic bottom waters. *Geochim Cosmochim Acta* 72:3703–3717.
15. Poulton SW, et al. (2015) A continental-weathering control on orbitally driven redox-nutrient cycling during Cretaceous Oceanic Anoxic Event 2. *Geol* 43:963–966.
16. Stookey LL (1970) Ferrozine – A New Spectrophotometric Reagent for Iron. *Analy. Chem.* 42:779–781.
17. Sperling EP, Halverson GP, Knoll AH, Macdonald FA, Johnston DT (2013) A basin redox transect at the dawn of animal life. *Earth Plan Sci Lett* 371-372:143–155.

18. Canfield DE, Raiswell R, JWestrich JT, Reaves CM, Berner RA (1986) The use of chromium reduction in the analysis of reduced inorganic sulfur in sediments and shales. *Chem Geol* 54:149–155.
19. Aller RC, Mackin JE, Cox RT Jr (1986) Diagenesis of Fe and S in Amazon inner shelf muds: apparent dominance of Fe reduction and implications for the genesis of ironstones. *Cont Shelf Res* 6:263–289.
20. Rue EL, Smith GJ, Cutter GA, Bruland KW (1997) The response of trace element redox couples to suboxic conditions in the water column. *Deep Sea Res Part I: Ocean Res Pap* 44:113–134.
21. Owens JD, Nielsen SG, Horner TJ, Ostrander CM, Peterson LC (2017) Thallium-isotopic compositions of euxinic sediments as a proxy for global manganese-oxide burial. *Geochim Cosmochim Acta* 213:291–307.
22. Ostrander CM, Owens JD, Nielsen SG (2017) Constraining the rate of oceanic deoxygenation leading up to a Cretaceous Oceanic Anoxic Event (OAE-2: ~94 Ma). *Sci Adv* 3:e1701020.
23. Rehkämper M, Halliday AN (1999) The precise measurement of Tl isotopic compositions by MC-ICPMS: Application to the analysis of geological materials and meteorites. *Geochim Cosmochim Acta* 63:935–944.
24. Nielsen SG, Rehkämper M, Baker J, Halliday AN (2004) The precise and accurate determination of thallium isotope compositions and concentrations for water samples by MC-ICPMS. *Chem Geol* 204:109–124.
25. Baker RGA, Rehkämper M, Hinkley TM, Nielsen SG, Toutain JP (2009) Investigation of thallium fluxes from subaerial volcanism – Implications for the present and past mass balance of thallium in the oceans. *Chem Geol* 73:6340–6359.
27. Caruthers AH, Smith PL (2012) Pliensbachian ammonoids from the Talkeetna Mountains (Peninsular Terrane) of Southern Alaska. *Rev de Paléo Gen* 11:365–378.
28. Caruthers AH, Gröcke DR, Smith PL (2011) The significance of an Early Jurassic (Toarcian) carbon-isotope excursion in Haida Gwaii (Queen Charlotte Islands), British Columbia, Canada. *Earth Plan Sci Lett* 307:19–26.
29. Caruthers AH, Smith PL, Gröcke DR (2013) The Pliensbachian-Toarcian (Early Jurassic) extinction, a global multi-phased event. *Palaeogeo Palaeoclim Palaeoecol* 386:104–118.
30. Percival LME, (2016) Osmium isotope evidence for two pulses of increased continental weathering linked to Early Jurassic volcanism and climate change. *Geol* 44:759–762.
31. Sell B, et al. (2014) Evaluating the temporal link between the Karoo LIP and climatic—biologic events of the Toarcian Stage with high-precision U-Pb geochronology. *Earth Plan Sci Lett* 408:48–56.
32. Ruhl M, et al. (2016) Astronomical constraints on the duration of the Early Jurassic Pliensbachian Stage and global climate fluctuations. *Earth Plan Sci Lett* 455:149–165.
33. Hermoso M, Le Callonnec L, Minoletti F, Renard M, Hesselbo SP (2009) Expression of the Early Toarcian negative carbon-isotope excursion in separated carbonate microfractions (Jurassic, Paris Basin). *Earth Plan Sci Lett* 277:194–203.

34. Hermoso M, et al. (2012) Dynamics of a stepped carbon-isotope excursion: Ultra high-resolution study of Early Toarcian environmental change. *Earth Plan Sci Lett* 319-320:45–54.
35. Hesselbo SP, Jenkyns HC, Duarte LV, Oliveira LCV (2007) Carbon-isotope record of the Early Jurassic (Toarcian) Oceanic Anoxic Event from fossil wood and marine carbonate (Lusitanian Basin, Portugal). *Earth Plan Sci Lett* 253:455–470.
36. Kemp DB, Coe AL, Cohen AS, Schwark L (2005) Astronomical pacing of methane release in the Early Jurassic period. *Nature* 437:396–399.
37. Littler K, Hesselbo SP, Jenkyns HC (2011) A carbon-isotope perturbation at the Pliensbachian-Toarcian boundary: evidence from the Lias Group, NE England. *Geol Mag* 147:181–192.
38. Jenkyns HC, Gröcke DR, Hesselbo SP (2001) Nitrogen isotope evidence for water mass denitrification during the early Toarcian (Jurassic) oceanic anoxic event. *Paleocean* 16:593–603.
39. Bodin S, et al. (2010) Toarcian carbon isotope shifts and nutrient changes from the Northern margin of Gondwana (High Atlas, Morocco, Jurassic): Palaeoenvironmental implications, *Palaeogeo Palaeoclim Palaeoecol* 297:377–390.
40. Woodfine RG, Jenkyns HC, Sarti M, Baroncini F, Violante C (2008) The response of two Tethyan carbonate platforms to the early Toarcian (Jurassic) oceanic anoxic event: environmental change and differential subsidence. *Sediment* 55:1011–1028.
41. Hesselbo SP, Pieńkowski G (2011) Stepwise atmospheric carbon-isotope excursion during the Toarcian Oceanic Anoxic Event (Early Jurassic, Polish Basin). *Earth Plan Sci Lett* 301:365–372.
42. Nielsen SG, et al. (2011) Thallium isotopes in early diagenetic pyrite – A paleoredox proxy? *Geochim Cosmochim Acta* 75:6690–6704.
43. McArthur JM, Algeo TJ, vd Schootbrugge B, Li Q, Howarth RJ (2008) Basinal restriction, black shales, Re-Os dating, and the Early Toarcian (Jurassic) oceanic anoxic event. *Paleocean* 23:PA4217.